# Electrical Transport Through a Single Nanoscale Semiconductor Branch Point

*Yi Cui[1,2], Uri Banin[2,3], Mikael T. Björk[2,4] & A. Paul Alivisatos[1,2*]*

Department of Chemistry, University of California and Materials Sciences Division, Lawrence Berkeley National Laboratory, Berkeley, California 94720, USA.

*To whom correspondence should be addressed. Email: alivis@berkeley.edu.

1 University of California, Berkeley. 2 Lawrence Berkeley National Laboratory. 3 Permanent address: Institute of Chemistry and the Center for Nanoscience and Nanotechnology, The Hebrew University of Jerusalem, Jerusalem 91904, Israel. 4 Current address: Solid State Physics/Lund University, P.O. Box 118, SE-221 00, Lund Sweden.

**ABSTRACT**. Semiconductor tetrapods are three dimensional branched nanostructures, representing a new class of materials for electrical conduction. We employ the single electron transistor approach to investigate how charge carriers migrate through single nanoscale branch points of tetrapods. We find that carriers can delocalize across the branches or localize and hop between arms depending on their coupling strength. In addition, we demonstrate a new single-electron transistor operation scheme enabled by the multiple branched arms of a tetrapod: one arm can be used as a sensitive arm-gate to control the electrical transport through the whole system.

Electrical transport through nanocrystals,[1] molecules,[2,3] nanowires[4,5] and nanotubes[6,7] display novel quantum phenomena. These can be studied using the single electron transistor approach to successively change the charge state by one, to reveal charging energies, electronic level spacings, and

1

coupling between electronic, vibrational, and spin degrees of freedom. The advent of colloidal synthesis methods that produce branched nanostructures[8,9] provides a new class of material which can act as conduits for electrical transport in hybrid organic-inorganic electrical devices such as light emitting diodes[10-12] and solar cells.[13,14] Already, the incorporation of branched nanostructures has yielded significant improvements in nanorod/polymer solar cells, where the specific pathways for charge migration can have a significant impact on device performance.[14] Progress in this area requires an understanding of how electrons and holes migrate through individual branch points, for instance do charges delocalize across the branches or do they localize and hop between arms. Here we employ the single electron transistor approach to investigate the simplest three dimensional branched nanostructure, the semiconductor tetrapod, which consists of a pyramidal shaped zincblende-structured "core" with four wurzite-structured arms projecting out at the tetrahedral angle.

Monodisperse CdTe tetrapods with arms 8 nm in diameter and 150 nm in length were synthesized as previously reported.[8] The tetrapods dispersed in toluene were deposited onto ~10 nm thick $Si_3N_4$ dielectrics with alignment markers and a back gate (see Supporting Information). A tetrapod spontaneously orients with one arm pointing perpendicularly away from the substrate and three arms projecting down towards the surface. Individual 60 nm-thick Pd electrodes were placed by EBL onto each of the three arms downwards so that there are four terminals (three arms and a back gate) as shown schematically in Fig. 1 top inset. Figure 1 bottom inset shows a typical scanning electron micrograph (SEM) of the devices. The center brighter spot is due to the fourth arm pointing up away from the substrate although its controlled breaking is possible.[15] The separation between the metal electrodes and the tetrapod branch point ranges from 30 to 80 nm in our devices. The devices were loaded into a $He^4$-flow cryostat for low-temperature (~5K) electrical measurements.

Typical curves of current (I) as a function of source-drain bias voltage (V) through arm pair 1-2 (Fig.1 bottom inset) at different back gate voltage ($V_g$) while keeping the third arm floating are presented in Fig.1 main panel. The I-V curves show a strongly suppressed conductance at small V and step-like increase of I at high V, suggesting single electron charging behavior. The size of the zero conductance

2

gaps could be changed reversibly by $V_g$. Pair 2-3 and 1-3 show similar behavior. Measurements are reproducible with time (Supporting Information Fig. 1). More than 20 working devices fabricated from 5 different independent processes have been measured. Their characteristics fall into two different categories (see below).
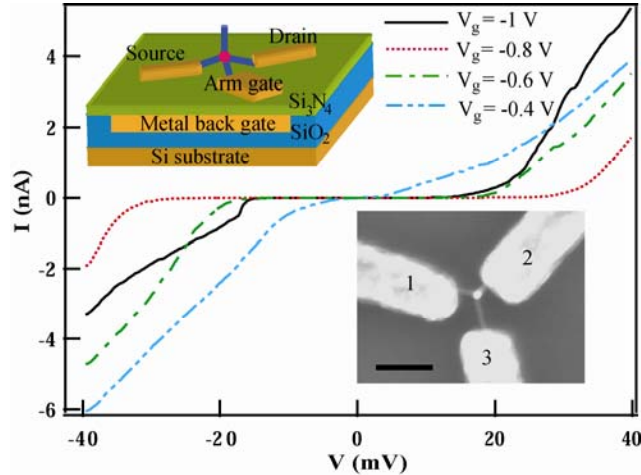


**Figure 1** Scheme of tetrapod single electron transistor and I-V. Main panel, I-V at different back gate voltages indicated with a different color and line style measured at T=5 K. Top inset, the device schematic structure, in which three arms of a tetrapod are contacted with small metal electrodes and the fourth arm points vertically away from the substrate. The red spot indicates the tetrapod branch point. Bottom inset, a SEM image of a tetrapod contacted with three Pd electrodes labeled as 1, 2, 3. Scale bar, 100 nm.

The differential conductance ($\partial I/\partial V$) as a function of V and $V_g$ for these two categories is plotted in Fig. 2a and c. Focusing now on Fig. 2a, the zero-conductance regions (purple) are now bound by higher conductance ones (light blue). Most notably, distinct from single dot charging, which has well-defined zero-conductance diamonds arranged one by one along the $V_g$ axis, the tetrapod shows many overlapping diamonds to the extent that the boundary of individual Coulomb diamonds exhibits a saw-tooth rather than smooth structure. This is a clear signature of single electron hopping in a system of weakly coupled quantum dots.[16] In the tetrapod, a coupled quantum dot system can form because the electron is transported through the arm-branch point-arm in series. Further support of this conjecture is

afforded by the addition energy, $E_{add}$ of ~30 meV obtained from the maximum size of V in the diamonds, which matches with the charging energy of the tetrapod branch point with a size ~10 nm. Here $E_{add} = E_c + \Delta E$, where $E_c$ is the Coulomb charging energy, $E_c = e^2/C$ and $\Delta E$ is the energy level spacing. For estimation of the order of magnitude, the capacitance C of a branch point can be approximated by sphere self-capacitance, $2\pi\varepsilon\varepsilon_0 D$, where $\varepsilon$ takes the average (4.5) of $Si_3N_4$ and vacuum dielectric constants, $\varepsilon_0$ is the vacuum permittivity, D is the branch point diameter. This gave an upper bound $E_c$ value of 60 meV since other capacitance contributions can reduce this value. The $\Delta E$ is ~ 5 meV and 45 meV from the effective-mass model for the holes and electron, respectively. Transport is most likely through valence band and does not contribute to $E_{add}$ significantly (see Supporting Information). The calculated $E_{add}$ is thus consistent with experiments. This addition energy can not be explained by charging the much larger whole tetrapod as a single quantum dot, which should display a charging energy of only a few meV. The observed value is also consistent with previous electrical transport[1] and scanning tunneling microscopy measurements[17] of quantum dots of size similar to the tetrapod core size. Other devices in the same category also give a narrow range of addition energies, 30 to 45 meV, further confirming it is mainly due to the branch point. A second addition energy scale observed in the data can be estimated from the separation between the adjacent saw-teeth, which is typically ~60 mV (between the two black lines in Fig. 2a), and when taking into account the gate coupling efficiency translates into a charging energy of ~10 meV, corresponding to the size of a single arm (estimated charging energy ~5 meV, see Supporting Information).[6]

Other mechanisms than electronic quantum dot and rod coupling are less likely to contribute significantly to the differential conductance spectra shown here. First, the vibration and twisting motions of tetrapods are at ~ GHz or μeV, which cannot account for the observed addition energy, although they might exert some effects on fine structure outside of the Coulomb diamonds. A second possibility is that surface localized surface defect states could play a role. The tetrapods here show little or no band edge luminescence and trap states within the band-gap act as non-radiative centers.[18] However, localized surface states are less likely to play a role in the transport measurements compared

4

to states that are more delocalized. Further, the Fermi level remains in the valence band (see Supporting Information) during measurements and defect states are less likely to play an important role at this energy although we observed sudden shifts of Coulomb charging diamonds along the $V_g$ axis once every few hours at 5 K. The measurements after temperature cycles still show similar sawtooth charging patterns with the same addition energy. To resolve this matter, we have investigated simple nanorods, which should not show coupling phenomena, but which do have surface states. Fig. 2b shows a similar measurement performed on a single quantum rod with dimension of 4 by 50 nm. Here a smooth set of Coulomb diamonds is seen indicating one addition energy scale characteristic of a single quantum dot. The value of the estimated charging energy is consistent with the rod dimension (see Supporting Information). This observation provides strong additional support for our assignment of the saw-tooth structure in the tetrapod case to single electron transport through the artificial molecule arm-branch point-arm system.
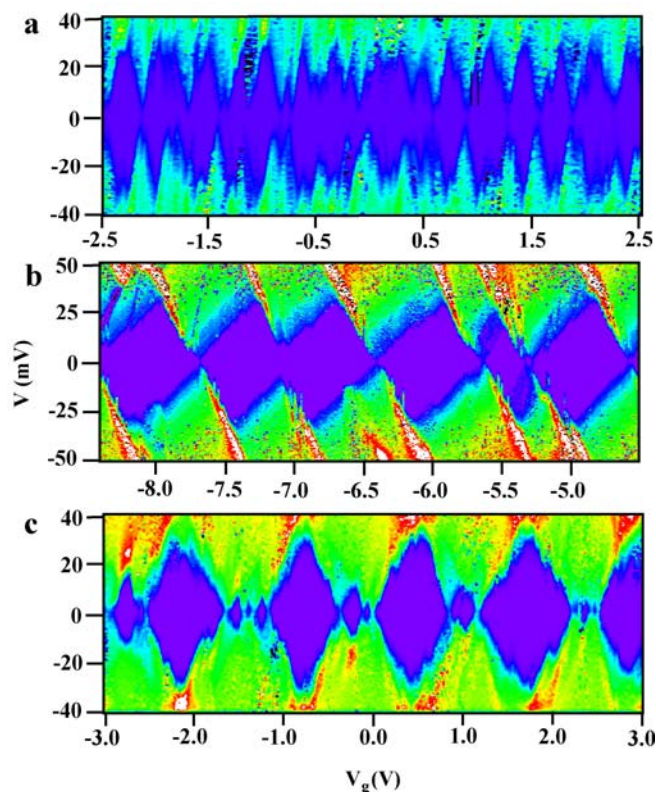


**Figure 2** Plots of $(\partial I/\partial V)$ as function of V and $V_g$ at T=5 K. **a**. A tetrapod showing hopping. The two black lines mark two of the sawteeth. **b**. A CdSe nanorod. The two sudden shifts along $V_g$ have been

corrected. The raw data is shown in Supporting Information Fig. 2. **c**. A tetrapod showing delocalization. The color scale: purple, zero; light blue 5 nS in **a**, green 25 nS in **b**, green 150 nS in **c**. The backgate coupling efficiency is different: ~16% in **a**, ~4% in **b** and **c**, due to the variation of dielectrics thickness.

Although 80% of the tetrapod devices exhibited sawtooth transport characteristics, in 20% we observed a different behavior as shown in Fig. 2c. Here a large diamond with an additional energy of ~30 meV and two or three small ones with additional energies of 3-15 meV alternate along the $V_g$ axis. These features can not be explained within a single-dot charging picture because $E_c$ and $\Delta E$ of the whole tetrapod as a dot are too small. Instead, these are expected for charge carrier delocalization within the whole tetrapod in the limit of strongly coupled arm-branch point-arm system similar to the lithographically patterned dots on two-dimensional electron gas.[19] Large diamonds correspond to the states with a large probability of a charge on the branch point and little on the arms since it is more confined; Small diamonds are the states with a large probability of a charge on the arms and little on the branch point since it is more spread out.

To further differentiate the two transport regimes in tetrapods, let us examine them more closely (Fig. 3a): 1). In the hopping case, the branch point and arms interact electrostatically with small tunnel conductance.[16] The charge carriers are localized on the individual branch points or arms and are incoherently transferred or hop between them. This regime can be modeled, to the simplest approximation, as three Coulomb charging energy ladders[20] (Fig. 3a left) connected in series which represent the arm-branch point-arm transport pathway. The other two arms can also cause some effect although their effect is not considered for qualitative analysis. Current can flow only if the charging levels line up within the window of V or the thermal fluctuation. 2). In the delocalization case, the coupling between the electronic states in the branch points and the arms is strong. The charge carrier can tunnel many times between the branch point and the arms and can be considered to coherently delocalize over the whole tetrapod. The Coulomb charging states can be modeled using a single energy

ladder (Fig. 3a right) formed by the hybridized bonding and antibonding states of the branch point and the arm charging states. Current can flow without the requirement of level lineup.
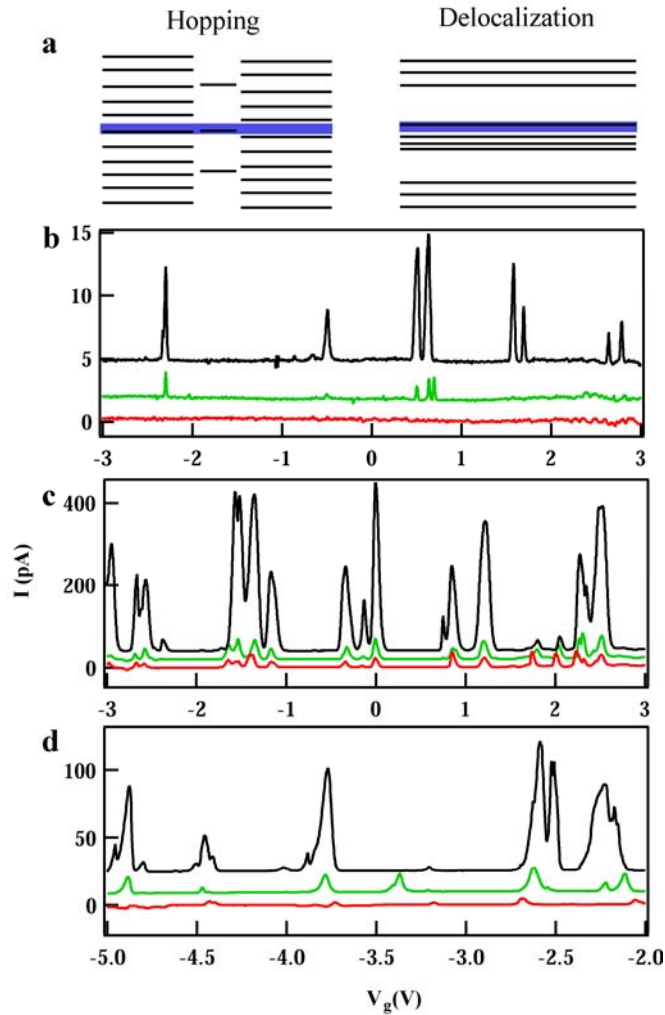


**Figure 3** Comparison of the hopping and delocalization couplings. **a**, Hopping and delocalization models. The blue stripes indicate V or the thermal energy window. **b** to **d**, Plots of I versus $V_g$ at T= 5 K and different V for hopping (**b**), delocalization (**c**) and nanorod (**d**). The red, green and black curves represents V= 1, 5, 10 mV in **b**; 0.5, 1, 5 mV in **c** and **d**. The curves are shifted in the vertical axis for clarity. **b** was taken from a device different from Fig. 2a. **c** and **d** were taken from the same device as Fig. 2c and b, respectively.

Bias or temperature dependence provides clear evidence to differentiate the two coupling mechanisms. Figure 3b plots I as a function of $V_g$ at different V values for the hopping case. Notably, when the bias is increased gradually from 1 mV to 10 mV, the number of Coulomb oscillation peaks

increases. This behavior can be explained by the three energy ladder model in the hopping limit. As the three energy ladders are randomly distributed, at small bias (1 mV, Fig. 3b red), the probability to have all three levels line up within the narrow energy window is small and thus the appearance of Coulomb oscillations peaks is sparse and appears stochastic.[20] Indeed in the gate scan range in Fig. 3b, there is no peak at all. At larger bias (5 mV, Fig. 3b green), the probability of line-up is increased and the peaks appear in the form of groups with a large separation between them, indicating capacitive coupling phenomena. When the bias is larger than the arm charging energy (10 mV, Fig. 3b black), there are always levels lining up within bias window for current flow. Thus the number of groups of peaks increases further. At even higher bias, the number of peaks within each group can increase due to conduction through excited states.

In contrast, the delocalization case shows very different V-dependent behavior (Fig. 3c). The Coulomb peaks appear also in groups but due to the hybridization of large and small charging energies, the peak number does not change when V is changed from 0.5, 1 to 5 mV, consistent with the single delocalized energy ladder. Compared with hopping and delocalization in tetrapods, similar measurements in single nanorods (Fig. 3d) show the same number of individual peaks at low bias except that there are peak splittings at high bias (black) due to excited state conduction. Temperature has a similar effect in controlling the transport window size and supports the above explanation (Supporting Information Fig. 3).

Weak hopping coupling with negligible inter-dot tunneling can be described by the orthodox theory of the Coulomb blockade.[21,22] The important parameters (capacitances, resistances) of the single electron transistor circuit have been extracted (Supporting Information Fig. 4) from the charge stability diamond plot as shown in Fig. 2a. Thus the weak coupling energy[16] in the hopping limit ($E_{\text{c-hopping}}$) between the

tetrapod branch point and the arm, can be calculated, $E_{c-hopping} = \dfrac{e^2}{C_{po\,int-arm}} \left( \dfrac{C_{po\,int} C_{arm}}{C_{po\,int-arm}^2} - 1 \right)^{-1}$, where e is

the electron charge, $C_{\text{point-arm}}$ is the capacitance between a branch point and a arm, $C_{\text{point}}$ and $C_{\text{arm}}$ is the total branch point and the total single arm capacitance, respectively. Given the $C_{\text{point-arm}}$, $C_{\text{point}}$ and $C_{\text{arm}}$

values of 2.4 aF, 5.3 aF and 26.7 aF from the transistor circuit, respectively (Supporting Information Fig. 4), we obtained an $E_{c\text{-hopping}}$ of ~3 meV. We note that the two arms coupled parallel to the transport pathway modify this coupling energy only in an insignificant manner.

In comparison, we also estimated the strong coupling energy in the delocalization limit ($E_{c\text{-delocalization}}$) for the plot shown in Fig. 2c. As a simple approximation, the coupling energy can be assigned as the spread range of the same group of Coulomb oscillation peaks as shown in Fig. 3c. Given a spread of 0.34 to 0.5 V in gate axis and a gate coupling efficiency, we obtained an $E_{c\text{-delocalization}}$ of 15- 20 meV, which is 5-7 times the estimated value of $E_{c\text{-hopping}}$. These coupling energy scales in tetrapod are one order of magnitude larger than those of lithographically patterned quantum dot molecules,[19] consistent with the much smaller size of the tetrapods.

There may be several sources for the interesting observation of both hopping and delocalization in tetrapods. Clearly this shows a variation of barrier heights at the arm-branch point-arm junctions between different tetrapod devices. A first possible source is strain induced by the mechanical bending of the arms close to the junction between the arms and the branch point. Mechanical strain can induce lattice distortion and thus change the band gap of a semiconductor.[23] Different degrees of bending will lead to band gap variations. Previous SEM studies provide clear evidence of arm bending in most due to capillary force attraction when the solvent dries during deposition on the substrate.[24] Recent atomic force microscopy and transmission electron microscopy studies also confirm that strain is most significant near the junction point of the tetrapod (private communications). To make a rough estimate of an energy barrier induced by mechanical bending, we simply treat the case as pure bending of a beam. Assuming a reasonable bending radius of curvature, R= 40 nm, the strain= r/R is determined to be 10%, where r is the radius of the arm. Taking the shear deformation potential[23] of CdTe ~1.4 eV, we get a 140 meV energy barrier, which is significant at cryogenic temperature. This is consistent with the fact that most of our samples show hopping coupling although the bending radius of curvature can vary widely in different tetrapods. The delocalization coupling requires that the arm bending is little with R > ~1μm, which can also happen in some tetrapods. Another possible source for the barriers is the

existence of stacking faults and change of growth angle at the arm-branch point interface, which may also vary between different tetrapods. Further experiments are required to clarify these two sources and are currently under investigation. For example, tuning the mechanism between the two coupling extremes continuously by controlling the mechanical deformation might be achievable by changing the interaction between substrate and tetrapod electrostatically, and/or by atomic force microscope manipulation.
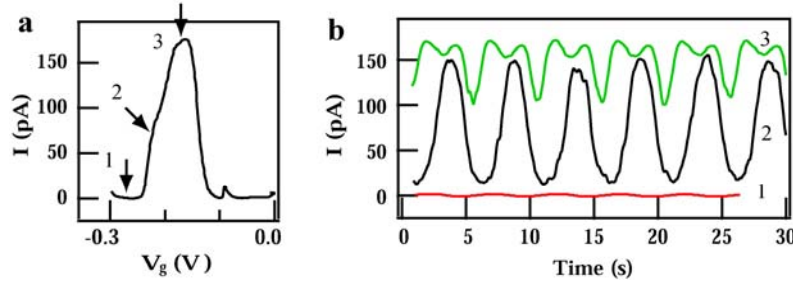


**Figure 4** Integrated tetrapod transistors at 5 K. **a**, I versus $V_g$ at V= 10 mV. The arrows indicate the three $V_g$ values for current at: 1, blockade; 2, half maximum; 3, peak. **b**, I versus time with V=10 mV and 0.2 Hz sinusoidal AC voltage applied to the third arm at the three $V_g$ values in **a**. The rms of the AC voltage is 40 mV for curve 1 and 2, 100 mV for 3. The I-V measurements through the third arm show a gap of 150 mV, presumably due to the defect formation during process and the AC voltage is small enough to avoid current leakage.

A coupled tetrapod also provides a unique integrated multi-terminal structure for new electrical device configurations. We have explored this opportunity by the third arm gating. We measured I across two of the arms at V=10 mV while scanning the back gate $V_g$ to locate a Coulomb oscillation peak as shown in Fig. 4a. We fixed V at 10 mV and $V_g$ at a specific value (position 1, 2, or 3) indicated by the arrow and applied 0.2 Hz AC voltage to the third arm. The current was recorded with time (Fig. 4b) and with voltage (Supporting Information Fig. 5). At position 1 of $V_g$, the current was in a blockaded state and modulating the arm gate gives little changes of current (Fig. 4 curve 1). In contrast, at position 2 where the current rises with $V_g$, the current can be changed by the arm gate from the peak value to almost zero. When $V_g$ is fixed at position 3, the modulation of current with the arm gate shows two

10

peaks within the 5 s period, consistent with two passes of the Coulomb oscillation peak in one period. From comparing the change of the back gate and arm gate voltage for the same amplitude of the current modulation, the arm gate coupling efficiency is estimated to be ~70% of that of the back gate efficiency. These preliminary studies suggest that the main gating mechanism is mainly through the third arm. Another gating mechanism from direct electrostatic interaction of the arm gate metal electrode and the tetrapod at a 30 nm distance would have a lower gating efficiency than the observed one and plays a less important role, although the future study is needed to subtract out its contribution in a quantitative way.

**Supporting Information Available:** Methods and supporting data. This material is available free of charge via the Internet at http://pubs.acs.org.

**References**

(1) Klein, D. L.; Roth, R.; Lim, A. K. L.; Alivisatos, A. P.; McEuen, P. L.. *Nature* **1997**, 389, 699-701.

(2) Park, J. et. al. *Nature* **2002**, 417, 722-725.

(3) Liang, W.; Shores, M. P.; Bockrath, M.; Long, J. R.; Park, H. *Nature* **2002**, 417, 725-729.

(4) Tans, S. J. et al. *Nature* **1997**, 386, 474-477.

(5) Bockrath, M. et al. *Science* **1997**, 275, 1922-1925.

(6) Cui, Y.; Duan, X.; Hu, J.; Lieber, C.M. *J. Phys. Chem. B* **2000**, 104, 5213-5216.

(7) Thelander, C. *et al. Appl. Phys. Lett.* **2003**, 83, 2052-2054.

(8) Manna, L.; Milliron, D. J.; Meisel, A.; Scher, E. C.; Alivisatos, A. P. *Nature Mater.* **2003**, 2, 382–385.

(9) Milliron, D. J. *et. al. Nature* **2004**, 430, 190-195.

(10) Colvin, V. L.; Schlamp, M. C.; Alivisatos, A. P. *Nature* **1994**, 370, 354.

(11) Coe, S.; Woo, W-K; Bawendi, M.; Bulovic, V. *Nature* **2002**, 420, 800-803.

(12) Tessler, N.; Medvedev, V.; Kazes, M.; Kan, S.; Banin, U. *Science* **2002**, 295, 1506-1508.

(13) Huynh, W. U.; Dittmer, J. J.; Alivisatos, A. P. *Science* **2002**, 295, 2425–2427.

(14) Sun, B.; Marx, E.; Greenham, N.C. *Nano Lett.* **2003**, 3, 961-963.

(15) Liu, H.; Alivisatos, A. P. *Nano Lett.* **2004**, 4, 2397-2401.

(16) van der Wiel, W. G. *et al. Rev. Mod. Phys.* **2003**, 75, 1-22.

(17) Banin, U.; Millo, O. *Ann. Rev. Phys. Chem.* **2003**, 54, 465-492.

(18) Nirmal, M.; Brus, L. *Acc. Chem. Res.* **1999**, 32, 407-414.

(19) Crouch, C. H; Livermore, C.; Westervelt, R. M.; Campman, K. L.; Gossard, A. C. *Appl. Phys. Lett.* **1997**, 71, 817-819.

(20) Ruzin, I. M.; Chandrasekhar, V.; Levin, E. I.; Glazman, L. I. *Phys. Rev. B* **1992**, 45, 13469-13478.

(21) Grabert, H.; Devoret, M. H. *Single charge tunneling: Coulomb blockade phenomena in nanostructures* (Plenum Press, New York, 1992), Chapter 1-3.

(22) Wasshuber, C. *Single electronics* (Spring-Verlag/Wien New York, 2001), Chapter 2.

(23) Mathieu, H.; Allegre, J.; Chatt, A.; Lefebvre, P.; Faurie, J. P. *Phys. Rev. B* **1988**, 38, 7740-7748.

(24) Y. Cui *et al. Nano Lett.* **2004**, 4, 1093-1098.